Chaos, Solitons and Fractals 140 (2020) 110217

Contents lists available at ScienceDirect

Chaos, Solitons and Fractals

Nonlinear Science, and Nonequilibrium and Complex Phenomena

journal homepage: www.elsevier.com/locate/chaos

Supersonic voidions in 2D Morse lattice

I.A. Shepelev[a], S.V. Dmitriev[b,c], A.A. Kudreyko[d], M.G. Velarde[e], E.A. Korznikova[f,b,*]

[a] National Research Saratov State University, Saratov 410012, Russia
[b] Institute for Metals Superplasticity Problems of RAS, Ufa 450001, Russia
[c] Institute of Molecule and Crystal Physics, Ufa Federal Research Center of RAS, Ufa 450054, Russia
[d] Department of Medical Physics and Informatics, Bashkir State Medical University, Ufa 450008, Russia
[e] Universidad Complutense de Madrid, Instituto Pluridisciplinar, Madrid 28040, Spain
[f] Ufa State Aviation Technical University, Ufa 450077, Russia

ARTICLE INFO

Article history:
Received 13 May 2020
Revised 28 July 2020
Accepted 17 August 2020
Available online 29 August 2020

PACS:
05.45.Xt
89.75.Fb

Keywords:
Crystal lattice
Atomistic simulations
Nonliner dynamics
Crowdions
Mass transfer

ABSTRACT

Dynamics of $M \times 1$-crowdion clusters ($M = 1$, 2 or 3) and vacancy clusters is analyzed in 2D triangular lattice with Morse interactions. Topological defects are created in the lattice by kicking three neighboring atoms in the three neighboring close-packed atomic rows along the rows. Initial velocity of the atoms in the inner row, v_{inn}, can be positive or negative, while the velocities of both atoms in the outer rows, v_{out}, are equal and positive. The case of $v_{inn} = v_{out}$ was analysed earlier and it was found that if the initial velocity is sufficiently large then a 3×1-crowdion cluster and a three-vacancy are formed. Two major effects are reported in the case of $v_{inn} \neq v_{out}$ analyzed here. (i) Due to the difference in the initial velocities, topological defects can be produced in the lattice with smaller initial energy than in the case of $v_{inn} = v_{out}$. (ii) In certain range of the initial velocities, a vacancy can appear at a distance of dozens interatomic distances from the initiation point, moving along the close-packed row with supersonic speed. Such moving vacancy is called voidion and mechanism of its formation and motion is revealed. Our results uncover new mechanisms of mass transfer by solitary waves in nonlinear lattices.

Introduction

Diffusion plays an important role in a number of processes taking place in metallic materials [1–3], contributing noticeably to the defect structure evolution, phase transitions and others. Diffusion is one of the mechanisms of mass transport in materials via thermally initiated random jumps of individual atoms. This mass transfer process is dominant in conditions close to thermal equilibrium [4–8]. Migration of vacancies or vacancy clusters is the main mechanism of diffusion in metals and alloys [3]. Interstitials have higher formation energy and their concentration in the conditions of thermal equilibrium is orders of magnitude smaller than that of vacancies [1,3]. Self-interstitials can form dumbbells or highly mobile crowdions [9–18].

In the far-from-equilibrium conditions, for example, during severe plastic deformation, ion implantation, irradiation, plasma surface treatment *etc.*, new mechanism of mass transfer by cooperative atomic displacements [19–25] or ballistic motion of atoms [26–29,29–33] can be realized.

A number of examples of mass transfer by cooperative atomic motion have been reported in the literature. Osetsky et al. have shown that clusters of interstitials are one-dimensionally (1D) mobile in fcc and bcc metals [19]. 1D motion of clusters was shown to be more energy profitable by comparison to 3D one [34] for the case of bulk diffusion. Matsukawa and Zinkle have observed experimentally one-dimensional fast migration of vacancy type prismatic loop in fcc gold [20]. The configuration of the glissile self-intertitial clusters is a prismatic dislocation loop, while sessile vacancy clusters form stacking fault tetrahedra [20]. Clusters of dozens of atoms (or vacancies) can exhibit 1D fast (subsonic) migration transporting the entire cluster with a mobility comparable to that of a single self-interstitial [19–22].

Ballistic mass transfer by supersonic crowdions and crowdion clusters is difficult to observe experimentally and it was studied with the aid of molecular dynamics simulations [26–29,29–33]. In the work [26] the notion of supersonic *N*-crowdions was introduced. In a supersonic *N*-crowdion not one but *N* neighboring atoms belonging to one close-packed atomic row move at a high speed at the same time along the row. In particular, supersonic 2-

* Corresponding author at: Institute for Metals Superplasticity Problems of RAS, Ufa 450001, Russia.
E-mail addresses: igor_sar@li.ru (I.A. Shepelev), dmitriev.sergey.v@gmail.com (S.V. Dmitriev), alexkudreyko@mail.ru (A.A. Kudreyko), mgvelarde@pluri.ucm.es (M.G. Velarde), ekorznikova@imsp.ru (E.A. Korznikova).

https://doi.org/10.1016/j.chaos.2020.110217
0960-0779/

and 4-crowdions were shown to be much more efficient in mass transfer as compared to the classical supersonic 1-crowdion because they travel longer distance having lower energy. It should be pointed out that supersonic 1- and 2-crowdions carry one interstitial, while supersonic 4-crowdion carries two interstitials [26]. It was shown that supersonic 2-crowdions can be initiated in fcc Pt from the surface by molecule bombardment [32]. With the help of the Frenkel-Kontorova model it was shown that bombardment by biatomic molecules requires less energy for mass transfer initiation than bombardment by molecules with a different number of atoms.

Supersonic crowdion clusters are decelerated due to the Cherenkov energy loss [35] and eventually they transform into subsonic ones. Subsonic crowdions can carry vibrational internal mode [36].

N-crowdions can be considered in 1D [30], 2D [37,38] or 3D [26,31,32] lattices. Natural generalization of *N*-crowdion is $M \times N$-crowdion in 2D lattice and $K \times M \times N$-crowdion in 3D lattice. Such crowdion clusters are excited by giving initial velocity to the corresponding blocks of atoms along a close-packed direction. Properties of $M \times N$-crowdions in 2D triangular lattice were addressed in [38]. Dynamics and stability of the subsonic $M \times 1$-crowdion clusters in 2D Morse crystal were analyzed in the works [37,38].

The opposite of crowdion is *voidion*, the former has excess density, while the latter refers to a rarefied region of a crystal. The term "voidion" has been used for the dilute-packed $< 110 >$ atomic rows collected in the form of a $1/2 < 110 > 110$ prismatic dislocation loop in fcc metals [20]. Cooperative transport on tungsten surface by a voidion mechanism triggered by high energy helium atom impact has been revealed by Mazilova et al. [39]. They have found that the surface voidions are extremely mobile with the velocity of atoms reaching a substantial portion of the sound velocity. A voidion (sparse one dimensional region) has been identified in simple cubic crystals of hard cubes [40]. In the Frenkel-Kontorova chain, voidions can exist as extended rarefied regions (kinks) only in the case when the inter-site interactions are sufficiently strong as compared to the on-site potential, otherwise a sharp vacancy is formed [30].

Voidions are studied much less then crowdions mainly because vacancies and vacancy complexes typically have lower mobility [19,20]. An extensive molecular dynamics study of clusters in collision cascades performed in [16] revealed the presence of both vacancy and interstitial clusters within the material, and a fraction of vacancy clusters was much smaller. In case of surface atomic migration the mechanism can change between hopping, crowdion, and exchange mechanism upon varying the strain state of the material [41]. Vacancies can form during surface impact by atoms in view of lower formation energy of vacancies by comparison to that of crowdions [42]. Presence of vacancy clusters near the surface was experimentally revealed in [39,43].

From the foregoing, the importance of studying the mechanisms of generation and movement of vacancies initiated by external impacts follows.

Here we strive to demonstrate the mechanism of formation of voidions under external impacts in the most transparent way. To do this, we choose a very simple model, namely a 2D triangular lattice with Morse interactions. 2D nonlinear lattices are often used for solving various physical problems [44–53]. In some cases, the triangular lattice can be used to describe the evolution of the structure in the (111) plane of the fcc lattice [48] or in the basal plane of the hcp lattice.

In Section 1 the simulation setup is described. Numerical results are presented in Section 2, and Section 4 concludes our work and discusses possible further work.

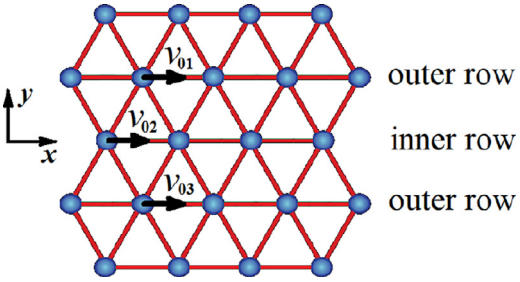

Fig. 1. Initial conditions used for excitation of 3×1-crowdions. Initial velocities v_{01}, v_{02}, and v_{03} are given to the three atoms in the adjacent close-packed atomic rows along the rows. Initial velocities of the outer rows are always equal and positive, $v_{01} = v_{03} > 0$, and will be referred to as v_{out}. Velocity of the inner row will be denoted as $v_{02} = v_{\text{inn}}$ and it can be positive or negative.

1. Simulation details

Triangular lattice having interatomic distance a is considered. Cartesian coordinate system x, y is used with the x axis aligned with the close-packed direction, see Fig. 1. Simulation cell, rectangular in shape, includes 100 close-packed atomic rows with 300 atoms in each row. Total number of atoms is thus $N = 3 \times 10^4$. The boundary conditions are periodic in both directions.

The interaction between atoms is determined using the Morse potential

$$U(r) = D(e^{-2\alpha(r-r_m)} - 2e^{\alpha(r-r_m)}), \tag{1}$$

where r is the distance between two atoms, D, α, and r_m are the parameters of the potential. The r_m parameter determines the position of the minimum of the function $U(r)$, the potential depth is D, and the bond stiffness depends on α. We choose such units of time, energy, and distance that the atom mass $M = 1$, $D = 1$, and $r_m = 1$. We fix the value $\alpha = 5$, for which the equilibrium interatomic distance is $a = 0.9881329$ for the cut-off radius of $5a$.

Morse potential is widely used in molecular dynamics modeling [54–64]. Girifalco and Weizer adjusted the Morse potential parameters for a number of fcc metals to the lattice parameter, sublimation energy, and bulk modulus [54]. For metals, the many-body potentials are more accurate, but calculations using the Morse potential are much faster due to its simplicity [55]. Morse parameters derived from the density functional calculations have been reported for the interaction of metals with graphene and silicene in [59]. Morse potential has been used in a recent study [62] to represent the interaction between workpiece and tool atoms in the simulation of cutting of Ni-based alloy. It is often used to describe the interactions at various interfaces [56,58,59,62,63]. The authors of the work [64] in their study of chaotic discrete breathers in triangular Morse lattice have set $D = 1/\alpha$ and called α a nondimensional parameter measuring the strength of nonlinearity of the Morse potential. In simulation of fcc metals D ranges from about 0.05 eV for alkali metals up to almost 1 eV for refractory metals such as Mo and W [54]. Interaction of metallic atoms with the three-coordinated carbon atoms is described by the Morse potential with $D = 0.363$ and 0.214 eV for Ni and Li, respectively [59].

The integration step in the molecular dynamics calculations is $\tau = 0.001$ time units.

For the subsequent discussion of numerical results, it is important to know the speed of sound in the considered crystal. For this purpose, we obtain linearized equations of atomic motion and solve the eigenvalue problem to determine the natural frequencies of oscillations for low-amplitude phonons with different wave vectors. Dispersion curves for longitudinal (L) and transverse (T) phonons are presented in Fig. 2 along the line $\Gamma - X$ of the first Brillouin zone. Phonon group velocity is $v_g = d\omega/dk$ and sound ve-

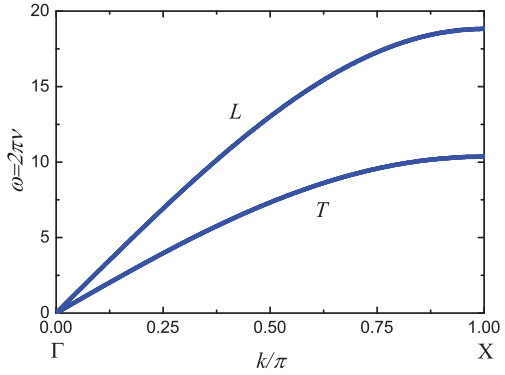

Fig. 2. Dispersion relations for the longitudinal (L) and transverse (T) phonons along the line Γ–X of the first Brillouin zone.

locity is the group velocity of waves with small k. Thus, we find that the longitudinal and transverse speeds of sound are

$$v_L = 8.98, \quad v_T = 5.18. \tag{2}$$

Note that a triangular lattice is elastically isotropic with sound velocities independent of the direction of propagation.

It is also important to discuss some characteristic energies in our simulations. Since we have set $D = 1$ in Eq. (1), the energy of single interatomic bond breaking is equal to 1. If an atom is removed from the lattice, a vacancy is formed with the energy roughly equal to 3, since this process requires breaking of three bonds. Formation of a Frenkel pair can be considered as a two-step process. First, a vacancy is created by removing one atom from the lattice, and then this atom is returned to the lattice at some distance from the vacancy. At the second step, bonds broken at the first step are restored, and the energy of the Frenkel pair is less than the energy of the vacancy. This energy depends on the distance between vacancy and interstitial and on the configuration of the interstitial. The latter can be in the form of a crowdion [Fig. 10(a), defect to the right of the bivacancy] or in the form of immobile interstitial [Fig. 10(b), defect to the right of the bivacancy]. We have performed relaxation of the lattice containing a Frenkel pair with a vacancy and interstitial at a large distance (20 interatomic distances) and found that the energy of vacancy-crowdion pair (vacancy-immobile interstitial pair) is 0.0130 (0.0126). The energy of a vacancy-crowdion pair is somewhat larger because, as it is well-known, this defect is unstable, while vacancy-immobile interstitial pair is in a local minimum of potential energy [37].

Main attention is paid to the process of the mass and energy transfer in the crystal by means of point defects, which are initiated by applying initial velocities simultaneously to three atoms in the three adjacent close-packed atomic rows along the rows, as shown in Fig. 1. Initial velocities for the outer rows are always positive and equal, $v_{01} = v_{03} > 0$, while the initial velocity of the atom in the inner row, v_{02}, can be positive or negative. Initial velocities of all other atoms are zero and initial displacements of all atoms in the computation cell are zero.

The simulations are conducted at zero temperature, meaning that thermal vibrations of atoms are not taken into account.

We will use the following notations for the initial velocities of the atoms in the outer and inner rows

$$v_{01} = v_{03} = v_{\text{out}}, \quad v_{02} = v_{\text{inn}}. \tag{3}$$

The initial kinetic energy of the ith excited atom ($i = 1, 2, 3$) is

$$E_{0i} = \frac{M v_{0i}^2}{2}. \tag{4}$$

Total energy of the system is

$$E_0 = E_{01} + E_{02} + E_{03}, \tag{5}$$

and it is conserved in time since the NVE thermodynamics ensemble is used (constant in time number of particles, volume and energy).

Molecular dynamic modeling is carried out using the atomic-molecular mass-parallel simulator (LAMMPS) software package [65]. The lattice was subjected to relaxation at zero temperature to obtain a minimum energy state before the simulation, thus finding the equilibrium lattice parameter.

We analyze the defect structure evolution scenarios for the initial velocities in the ranges $-4 \le v_{\text{inn}} \le 12$ and $7 \le v_{\text{out}} \le 14$. The case of equal velocities $v_{\text{out}} = v_{\text{inn}}$ has been considered in our previous works [29,37], but here we focus on the case of $v_{\text{out}} \neq v_{\text{inn}}$.

As can be seen from Eq. (4), at an initial velocity of, say, 10, the excited atom receives kinetic energy equal to 50, which is three orders of magnitude greater than the energy of the Frenkel pair in our model. Nevertheless, this initial energy can be considered small if it is compared with the energy of fast neutrons (0.1-1 MeV) emerging from a nuclear reactor. The energy of fast neutrons is five to six orders of magnitude higher than the energy of point defects in reactor materials [22].

2. Numerical results

The main goal of this work is to study the defect structures arising from the excitation of three atoms with different initial velocities v_{inn} and v_{out}. The initial excitation of atoms leads to their displacement from their equilibrium positions. Propagation of the excitation and the structure of emerging defects depend on two main factors. The first is the amount of energy E_0 given to the atoms. If the kinetic energy transferred to the atoms at $t = 0$ is insufficient to create a topological defect, then the solitary waves called focusons are initiated, after attenuation of which the structure of the crystal lattice is completely restored. If the initial energy is sufficient for overcoming the potential barrier of the formation of topological defects, then the Frenkel pairs appear in the form of vacancies and interstitial atoms (crowdions). The second important factor analyzed in this work is the ratio of the initial atomic velocities v_{inn} and v_{out}.

2.1. Compressive soliton (focuson)

Firstly we consider the case when total energy E_0 initially given to the lattice is insufficient for the formation of topological defects.

By setting initial velocities $v_{\text{inn}} = 4.5$ and $v_{\text{out}} = 8$ ($E_0 = 74.1$), the 3 × 1-focuson is initiated, as shown in Fig. 3, where atoms are colored according to their total energy: dark blue atoms are in the ground state with minimal energy and red color is used for the atoms with the highest energy. Initial state is shown in (a), three focusons propagating along the close-packed rows can be seen in (b), and (c) shows the defect-free lattice after the energy of the initial excitation is dissipated into heat.

Another representation of the 3 × 1-focuson motion is given in Fig. 4. The atoms in the three initially excited atomic rows are numbered by the index n with $n = 0$ for the excited atoms. Let the components of the displacement vector of the atoms are $(\Delta X_n^{\text{inn}}, \Delta Y_n^{\text{inn}})$ and $(\Delta X_n^{\text{out}}, \Delta Y_n^{\text{out}})$ for the inner and outer atomic rows, respectively. In Fig. 4, normalized displacements of the atoms, $x_n = \Delta X_n/a$, in (a) outer and (b) inner atomic rows are shown as the functions of time for $v_{\text{inn}} = 4.5$ and $v_{\text{out}} = 8$ (the case presented in Fig. 3). It can be seen that in the outer and inner rows the atoms do not reach the top of the potential barrier, which is at $x_n = 0.5$. All atoms eventually return to their initial positions, $x_n = 0$. In the three atomic rows the compressive solitary waves

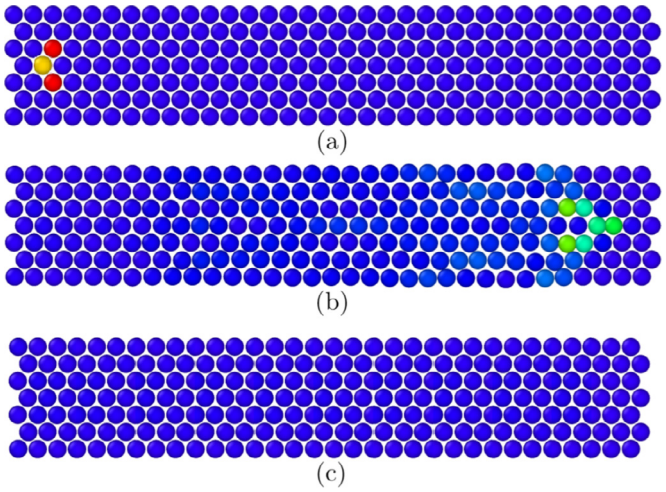

Fig. 3. Propagation of 3 × 1-focuson initiated with velocities $v_{inn} = 4.5$ and $v_{out} = 8$, $E_0 = 74.1$ (regime A in the regime map shown in Fig. 11). Dark blue atoms have minimal energy and red atoms have the highest energy. (a) Initial state with three atoms kicked to the right along the close-packed rows. (b) Propagation of the focusons in three neighboring rows. (c) Final defect-free structure after the energy of the initial kick is dissipated into heat. (For interpretation of the references to colour in this figure legend, the reader is referred to the web version of this article.)

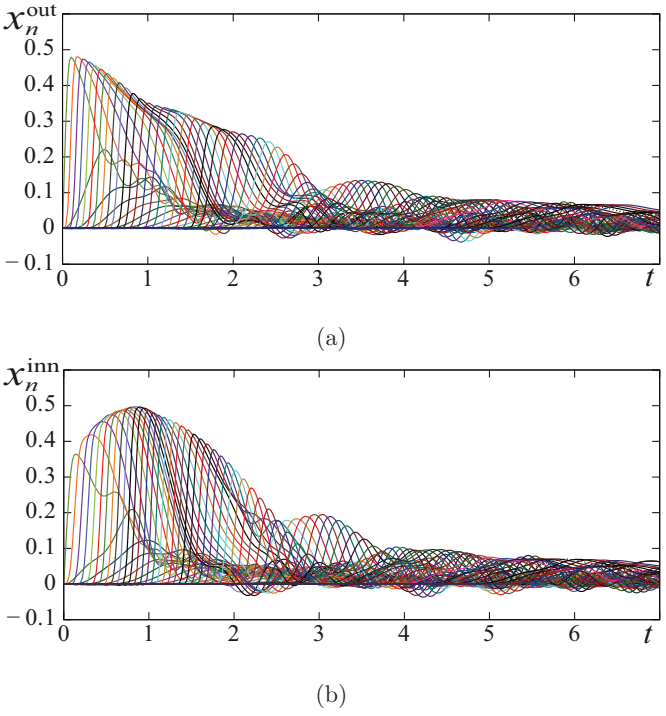

Fig. 4. Displacements of atoms normalized to the interatomic distance, $x_n = \Delta X_n/a$, as the functions of time for the initial velocities $v_{inn} = 4.5$ and $v_{out} = 8$, $E_0 = 74.1$. The result in (a) is for the outer rows, while in (b) for the inner row. Solitary waves or focusons are formed in both types of rows. Focusons transfer energy, but not mass, and this type of dynamics is called regime A (see the regime map in Fig. 11).

(focusons) are formed. They slow down due to the Cherenkov radiation [35].

One may wonder why such a high energy ($E_0 = 74.1$), as compared to the bond breaking energy $D = 1$, is not enough to create a topological defect. The reason is that the initial energy spreads over many atoms. Looking at Fig. 4, one can recognize that passing focuson lifts many atoms to almost top of the potential barrier close to $x_n = 0.5$. This is, however, a cooperative motion and atoms

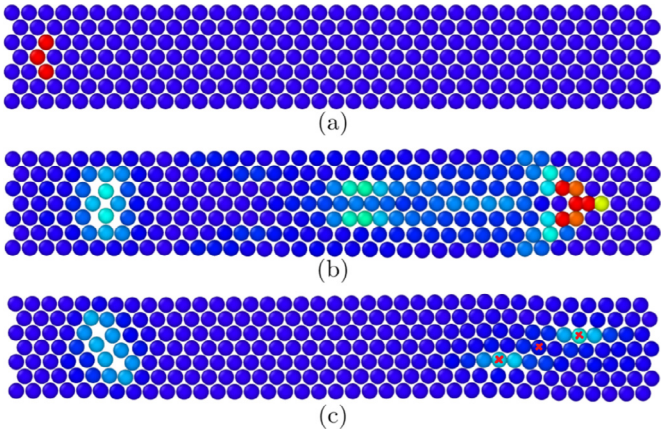

Fig. 5. Initiation and propagation of the 3 × 1-crowdion for the initial velocities $v_{inn} = 8$ and $v_{out} = 10$, $E_0 = 132$ (regime B in the regime map in Fig. 11). Dark blue atoms have minimal energy and red atoms have the highest energy. (a) At $t = 0$ three atoms are excited (red atoms at left). (b) Transformation of the supersonic 3 × 1-crowdion into subsonic 3 × 1-crowdion. This transition is accompanied by the emission of the 3 × 1-focuson, which is at right. Later the focuson disappears leaving no topological defects. A non-relaxed three-vacancy is formed at left. (c) Subsonic 3 × 1-crowdion moving from the left to the right. Interstitials are marked by red crosses. At left a relaxed three-vacancy is seen. (For interpretation of the references to colour in this figure legend, the reader is referred to the web version of this article.)

do not lose their neighbors during the focuson propagation. After dissipating energy into heat, all atoms reach their initial positions without formation of topological defects.

Interestingly, in the inner row maximal deviations of the atoms from equilibrium grow in time up to $t \approx 1$ and then start to decrease. This means that the atoms of the inner row obtain energy from the atoms of the outer rows, the latter ones received larger initial energy. In other words, the energy dissipated by the focusons moving in the outer rows is pumped into the focuson moving in the inner row. The possibility of energy exchange between atomic rows during the propagation of M × 1-focusons or M × 1-crowdions is important for future discussion.

Focusons transport only energy but not mass and this type of dynamics will be called regime A. This regime is realised within the blue portion of the (v_{inn}, v_{out}) plane shown in Fig. 11.

2.2. Supersonic crowdion

Scenario of supersonic 3 × 1-crowdion formation and propagation discussed in this section is called regime B (yellow area of Fig. 11).

The initial velocity is beyond the threshold level of atomic bond breaking and the atoms obtain enough energy for a Frenkel type reaction when pairs of point defects of opposite signs emerge (vacancies and interstitials). More precisely, in this case three vacancies and three interstitials embedded in the close-packed atomic rows are formed. The interstitials are highly mobile and they start to propagate along the close-packed rows with the velocity exceeding the speed of sound and later transform into subsonic crowdions being decelerated due to the energy losses. Moving interstitials transfer not only energy but also mass.

Excitation and propagation of the 3 × 1-crowdion with $v_{out} = 10$ and $v_{inn} = 8$ ($E_0 = 132$) is shown in Fig. 5, where atoms are colored according to their total energy. Dark blue atoms have minimal energy, while red atoms have maximal energy. At $t = 0$, see panel (a), the kinetic energy is given to the three atoms having red color. In (b) the transformation of supersonic 3 × 1-crowdion into subsonic one can be seen. During this process a 3 × 1-focuson is emitted (it is at right) and later it disappears after energy dissi-

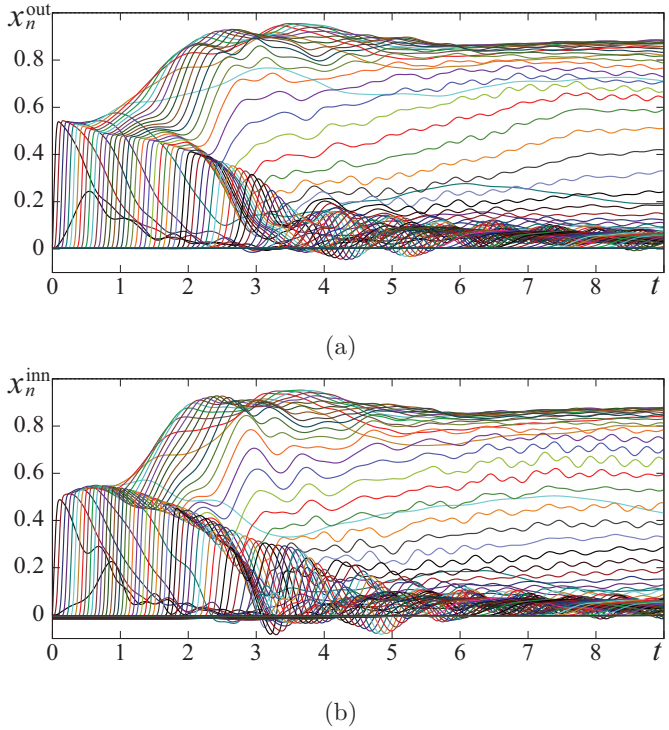

Fig. 6. Displacements of atoms normalized to the interatomic distance, $x_n = \Delta X_n/a$, as the functions of time for the initial velocities $v_{inn} = 8$ and $v_{out} = 10$, $E_0 = 132$. The result in (a) is for the outer rows, while in (b) for the inner row. Supersonic 3×1-crowdion is formed which transforms into the subsonic one at about $t = 2.5$. Atoms overcome the potential barrier at $x_n = 0.5$ and move to the next equilibrium position at $x_n = 1.0$. 3×1-crowdion transfers energy and mass, and this type of dynamics is called regime B (see the regime map in Fig. 11).

pation into heat. At left, a non-relaxed three-vacancy is formed at the position about three interatomic distances to the right from the initiation point. In (c) at left, a relaxed three-vacancy and at right, the subsonic 3×1-crowdion moving to the right are formed. The three interstitial atoms are marked with red crosses.

The same process is shown in Fig. 6 by the displacements of the atoms as the functions of time for (a) outer and (b) inner atomic rows. The 3×1-crowdion first propagates with the supersonic speed and, at $t \approx 2.5$ transforms into the subsonic crowdion cluster. The atoms cross the potential barrier located at $x_n = 0.5$ and move further to the new interatomic position at $x_n = 1.0$. In contrast to the case shown in Fig. 4, here some atoms lose their neighbors, which leads to the formation of topological defects.

Here again, we note that in the inner row [see Fig. 6(b)] the maximal displacements of the atoms in the supersonic regime of motion increase in time up to $t = 0.6$ and then start to decrease. This is due to the energy transfer from the outer rows to the inner row, which was initially excited with lower energy.

Formation of 3×1-crowdion and three-vacancy is the regime B, which is realised within the yellow portion of the (v_{inn}, v_{out}) plane shown in Fig. 11.

2.3. Voidion

The regimes A and B described above can only be realized with relatively small differences in the initial velocities v_{inn} and v_{out}. If the initial velocity in the middle row is relatively small, or even has the opposite direction, then the defect structure evolution becomes more complicated and, typically, a vacancy appears rather far from the initiation point. A variety of such structure transformations will be called regime C, which is shown by pink color in the regime map Fig. 11.

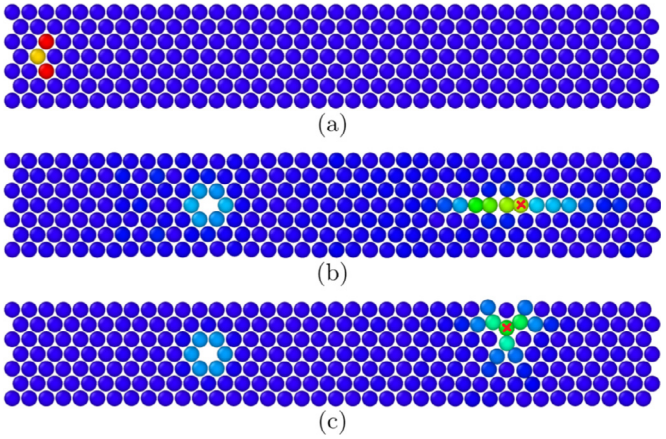

Fig. 7. Formation of defects for the initial velocities $v_{inn} = 0.5$ and $v_{out} = 9$ for the regime C in the regime map in Fig. 11. Dark blue atoms have minimal energy and red atoms have the highest energy. (a) The initial state. (b) A vacancy formed 10 interatomic distances away from the initiation point and a subsonic 1×1-crowdion, which appears from the decelerated supersonic 1×1-crowdion (not shown here). (c) Unstable subsonic 1×1-crowdion leaves the close-packed atomic row. The interstitial atom in (b) and (c) is marked with red cross. (For interpretation of the references to colour in this figure legend, the reader is referred to the web version of this article.)

It is natural to call vacancy that appears very far from the initiation point *voidion*, as it will be rationalized in Section 3.

At first, let us consider relatively small velocity of the outer rows, $v_{out} = 9$, with even much smaller velocity $v_{inn} = 0.5$, for which initial energy is $E_0 = 81.1$. Defect structure formed in this case is shown in Fig. 7. Strikingly, as it is seen in (b), a vacancy and an interstitial appear only in the inner row, while most of the energy was given to the outer rows. This happens because energy from the outer rows is transferred into the inner row in an amount sufficient to overcome the potential barrier for the Frenkel pair formation. Another counter intuitive result is the appearance of the vacancy at a distance of $10a$ from the excited atom. The mechanism of voidion motion will be discussed later. Thus, in this example, we have formation of a voidion and a supersonic 1×1-crowdion which transforms into a subsonic crowdion. It is well known that the 1×1 subsonic crowdion is unstable [37] and the interstitial leaves the close-packed atomic row, as shown in Fig. 7(c).

Now we take somewhat larger velocity v_{out} and *negative* velocity v_{inn}.

In Fig. 8 the case of $v_{inn} = -3$ and $v_{out} = 11$ with $E_0 = 125$ is considered. The initial state is not shown. In (a), at left we see the formation of a bivacancy in the outer rows. At right a vacancy in the inner row and a subsonic 3×1-crowdion are observed. The 3×1-crowdion and closely located vacancy are mutually attractive quasi-particles of opposite topological charge. Annihilation of the vacancy with one of the interstitial atoms results in the formation of inclined 2×1-crowdion, as shown in (b). Similar effect of changing the crowdion propagation direction has been earlier reported in [32].

Let us further increase the velocity v_{out} keeping negative value for v_{inn}.

The case of $v_{inn} = -3$ and $v_{out} = 12$ with $E_0 = 148.5$ is shown in Fig. 9. The initial stage of motion of the two supersonic 1×1-crowdions in the outer rows is not shown here. In (a) at left a bivacancy in the outer rows is formed. In the middle, a vacancy and a subsonic 1×1-crowdion are about to annihilate in the inner row. At right, a vacancy in the inner row and a subsonic 3×1-crowdion

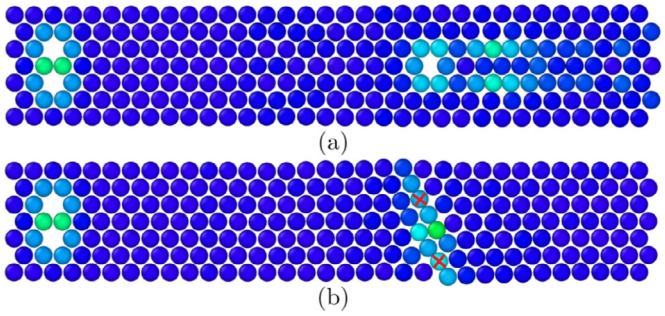

Fig. 8. Formation of the inclined 2 × 1-crowdion and bivacancy for the initial velocities $v_{inn} = -3$ and $v_{out} = 11$ with $E_0 = 125$ for the regime C in the regime map in Fig. 11. Color coding is same as in previous similar figures. (a) At left a bivacancy in outer rows is formed, while at right a vacancy in the inner row and a subsonic 3 × 1-crowdion appears. (b) Annihilation of a vacancy with an interstitial of the 3 × 1-crowdion results in the formation of the inclined 2 × 1-crowdion. The two interstitials are marked with red crosses. (For interpretation of the references to colour in this figure legend, the reader is referred to the web version of this article.)

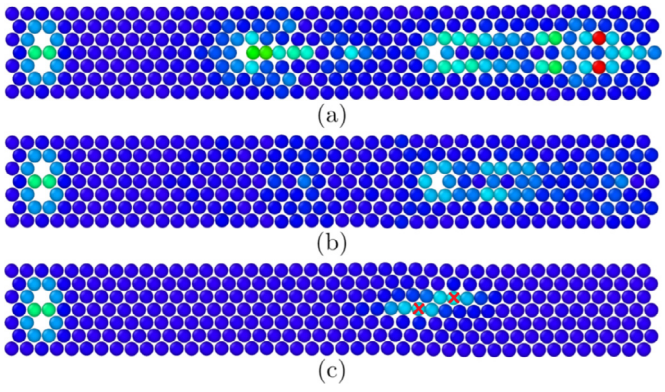

Fig. 9. Formation of the 2 × 1-crowdion and bivacancy for the initial velocities $v_{inn} = -3$ and $v_{out} = 12$ ($E_0 = 148.5$), which is regime C in the regime map in Fig. 11. Color coding is same as in previous similar figures. (a) At left, a bivacancy in the outer rows is seen. In the middle, a vacancy and a 1 × 1-subsonic crowdion are about to annihilate. At right, a vacancy in the inner row and a 3 × 1-subsonic crowdion are about to react. (b) Bivacancy at left remains, while the point defect in the middle annihilate. At right, the vacancy in the inner row and the 3 × 1-subsonic crowdion get closer due to mutial attraction. (c) Bivacancy is at left and the subsonic 2 × 1-crowdion is formed as the result of reaction between the vacancy in the inner row and the 3 × 1-subsonic crowdion. Interstitials are marked by red crosses. (For interpretation of the references to colour in this figure legend, the reader is referred to the web version of this article.)

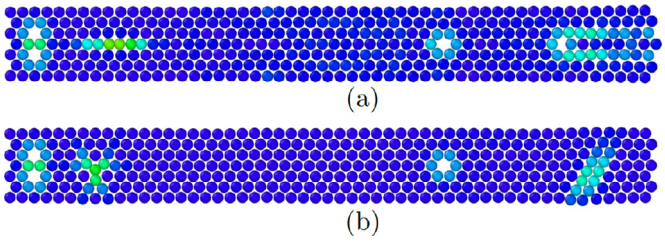

Fig. 10. Defect structure evolution for the case of $v_{inn} = -3$ and $v_{out} = 14$ ($E_0 = 200.5$), the regime C in the regime map in Fig. 11. Color coding is same as in the previous similar figures. (a) From the left to the right: a bivacancy in the outer rows; an unstable subsonic 1 × 1-crowdion in the inner row; a vacancy in the inner row; closely placed vacancy in the inner row and subsonic 3 × 1-crowdion, that are about to react. (b) From the left to the right: a bivacancy in the outer rows; an immobile interstitial formed from the unstable subsonic 1 × 1-crowdion; a vacancy in the inner row; inclined subsonic 2 × 1-crowdion formed from the vacancy in the inner row and subsonic 3 × 1-crowdion.

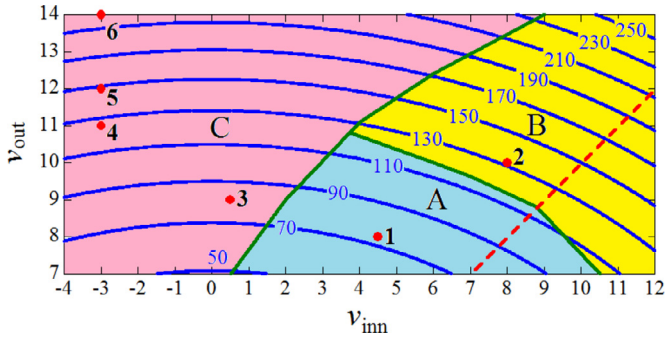

Fig. 11. Plane of initial velocities (v_{inn}, v_{out}) separated into the regions A, B, and C colored blue, yellow, and pink, respectively, where the corresponding dynamical regimes are realized. Dark blue contour lines show the values of energy E_0 given to the system. Red dashed line is $v_{inn} = v_{out}$. Excitation within the regime A does not produce topological defects because the initial velocities are too small and the difference in the initial velocities v_{inn} and v_{out} is also relatively small. In the regime B, which is close to the case of $v_{inn} = v_{out}$ and the initial energy is sufficiently large, 3 × 1-crowdion and three-vacancy are formed. In the regime C, where v_{out} is considerably greater than v_{inn}, the energy transmission from the outer rows to the inner row should be taken into consideration. In regime C Frenkel pairs do appear, and besides, a vacancy is typically formed far from the initiation point. (For interpretation of the references to colour in this figure legend, the reader is referred to the web version of this article.)

are about to react with the formation of a 2 × 1-crowdion, which can be seen in (c). As one can see, a 3 × 1-crowdion plus a vacancy can create either inclined 2 × 1-crowdion, as in Fig. 8(b), or a 2 × 1-crowdion moving along x-axis, as in Fig. 9(c). A distinct feature of this regime is that the initial energy of the outer rows is already so large, that, at the initial stage, the movement of the supersonic 1 × 1-crowdions in the outer rows induces the short-lived subsonic 1 × 1-crowdion in the inner row due to the energy exchange between rows. At the same time, one can observe the formation of a vacancy in the inner row which annihilates with the subsonic 1 × 1-crowdion in the inner row.

Finally, we take $v_{inn} = -3$ and $v_{out} = 14$ ($E_0 = 200.5$) and present the result in Fig. 10. Again, we skip the regime of propagation of the two supersonic 1 × 1-crowdions in the outer rows and show only the regime with subsonic crowdions after the energy exchange between the rows took place. Fig. 10(a) should be compared to Fig. 9(a). They are similar with some important differences. In both cases, at left one has a bivacancy in the outer rows. Also in both cases at right a vacancy in the inner row and closely placed subsonic 3 × 1-crowdion appear, and they are about to react with each other with the formation of a subsonic 2 × 1-crowdion, inclined as in Fig. 10(b) or not inclined, as in Fig. 9(c). The difference is that vacancy and interstitial in the inner row in Fig. 9(a) are close to each other and they annihilate, while in Fig. 10(a) they are far away and the interstitial transforms into an immobile defect and the vacancy remains in the system. Remarkably, the mono-vacancy is almost 40 interatomic distances away from the initiation point. In what follows, the mechanism of vacancy propagation in the form of a voidion will be discussed.

2.4. Discussion of the regime map

Now we turn to the discussion of the regime map presented in Fig. 11 on the (v_{inn}, v_{out}) plane. Dark blue contour lines show the values of initial energy E_0. Red dashed line is $v_{inn} = v_{out}$.

Blue portion of Fig. 11 corresponds to the regime A and the red point 1 indicates the initial velocities used to plot Fig. 3. Here initial energy is insufficient for the formation of point defects and 3 × 1-focuson is formed. After attenuation of the focuson all atoms come back to their initial equilibrium positions.

Yellow portion of Fig. 11 corresponds to the regime B and the red point 2 stands for the initial velocities considered in Fig. 5. Here initial energy is large enough for the formation of point defects and 3 × 1-crowdion is formed, which first propagates with the speed exceeding the speed of sound and then transforms into subsonic 3 × 1-crowdion. Together with the 3 × 1-crowdion a three-vacancy is formed. The line that separates the regimes A and B is at the level of initial energies $100 < E_0 < 120$.

Both regimes A and B are observed around the line $v_{inn} = v_{out}$, i.e., when the difference in the initial velocities of the atoms in the outer and inner rows is not too large.

Pink portion of Fig. 11 corresponds to the regime C where point defects do appear and, in many cases, a vacancy is formed rather far from the initiation point. The line separating this regime from the regimes A and B is roughly parallel to the line $v_{inn} = v_{out}$. The difference of the initial velocities v_{inn} and v_{out} is large in the regime C and the energy exchange between the outer rows and the inner row plays a very important role.

Importantly, in the regime C, point defects are formed at much smaller initial energy than in the regime B. Even $E_0 = 50$ is enough for the formation of single Frenkel pair following the scenario presented in Fig. 7 (red point 3). As it was already mentioned, regime B is realized for $E_0 > 100$.

Red points 4, 5, and 6 indicate the initial values of the velocities v_{inn} and v_{out} used to produce Figs. 8, 9, and 10, respectively. In all these cases a vacancy appears in the inner row pretty far from the initiation point. In some cases (Figs. 8 and 9) the vacancy annihilates with an interstitial, but in other cases, e.g., in Fig. 10, it remains in the system.

We come to the question how a vacancy can appear so far from the initiation point and what is the mechanism of its generation and motion. In the next Section this mechanism is discussed.

3. Mechanism of voidion formation

The reason for the emergence of a vacancy at a large distance from the initiation point is an open question and requires a detailed analysis. We should take into account that this scenario is realized only when v_{inn} is considerably smaller than v_{out} or even have the opposite sign. Obviously, the energy exchange between the outer rows and the inner row should be considered.

Our idea is that the motion of the two supersonic 1 × 1-crowdions in the outer rows brings the atoms of the inner row at the top of the potential barrier, i.e., the atoms of the inner row are displaced by about $x_n = 1/2$. From the top of the barrier the atoms of the inner row, depending on small deviations, can either return to their original positions or move to the neighboring equilibrium positions.

In line with this assumption, we introduce the notion of an extended vacancy or voidion. The formation and possible ways of relaxation of a voidion are shown in Fig. 12. In (a) one has a vacancy in the inner row. In (b), a voidion is shown, which is produced from the vacancy shown in (a) by shifting 24 atoms of the inner row, which are to the right from the vacancy, by exactly half the interatomic distance to the left, $x_n = -1/2$ for $n = 1, \ldots, 24$. Thus the vacancy is transformed into two well separated rarefied regions. The shifted 24 atoms are at the top of the potential barrier in the state of unstable equilibrium. Depending on small perturbations in the atomic positions the atoms can slide either to the right or to the left toward energy minimum positions. If all unstable atoms slide to the right, the vacancy appears at its original position, see in (c). On the other hand, if all the atoms slide to the left, then the vacancy is formed 24 atoms away from its initial position, see in (d). If the left half of the unstable atoms move to the left and the right half to the right, then the vacancy appears in the middle, see in (e). If the left half of the unstable atoms move to the right and the right half to the left, then two vacancies and an interstitial between them are formed, see in (f). Note that Fitzgerald has considered a double sine-Gordon model to introduce shallow minimum at the top of the on-site potential barrier to stabilize the atoms of voidion in (b) [66].

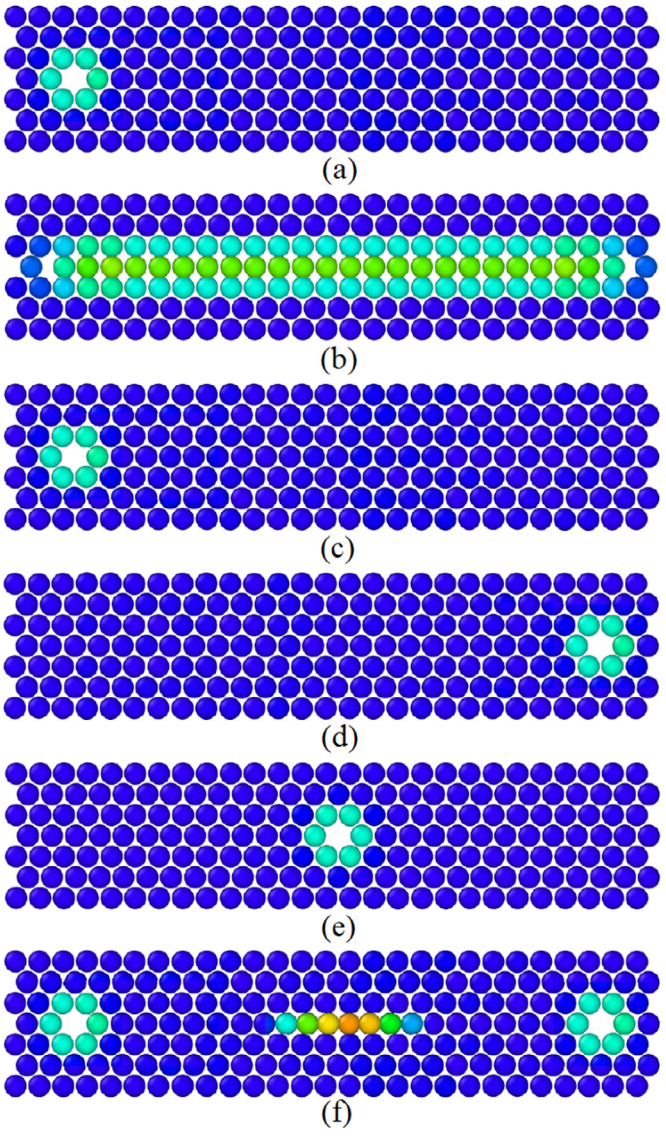

Fig. 12. Schematic of voidion formation and relaxation. Color coding is same as in the previous similar figures (a) A vacancy in the inner row. (b) A voidion produced from the vacancy shown in (a) by shifting 24 atoms in the inner row to the left by $x_n = -1/2$. All shifted atoms are in unstable equilibrium positions and with equal probability they can move either to the right or to the left, toward the energy minimum positions. (c) The result of voidion relaxation when all 24 unstable atoms move to the right by the distance $x_n = 1/2$. A vacancy appears at the original place. (d) All 24 unstable atoms move to the left by the distance $x_n = -1/2$. A vacancy appears at the right end of the voidion. (e) First 12 unstable atoms move to the left by $x_n = -1/2$ and the rest unstable atoms move to the right by $x_n = 1/2$. A vacancy emerges in the middle of the voidion. (f) First 12 unstable atoms move to the right by $x_n = 1/2$ and the rest unstable atoms move to the left by $x_n = -1/2$. Two vacancies at the voidion's ends and a crowdion between them are formed.

Having the discussion related to Fig. 12 in mind, one can offer the following explanation to the appearance of a vacancy far from the initiation point in the case when v_{out} is sufficiently large and v_{inn} is considerably smaller or even having the opposite sign, in other words, in the region C of the regime map, Fig. 11.

Two interstitials propagating along the outer rows with supersonic speed drag the atoms of the inner row to the positions close

to the unstable equilibrium. A large group of unstable atoms in the inner row can cooperatively slide in the negative direction of the x-axis, which leads to a jump of the vacancy to a large distance to the right. This process is possible due to the large difference in the velocities of motion of the atoms in the outer rows (supersonic motion) and the slow relaxational motion of the unstable atoms in the inner row.

4. Conclusions

Employing molecular dynamics simulations we have performed the study of point defects in 2D Morse lattice created by giving initial momentum to three neighboring atoms in three neighboring atomic rows along the rows, see Fig. 1. Atoms in the outer rows had equal and positive initial velocity v_{out}, while the initial velocity of the atom in the inner row, v_{inn}, could be positive or negative.

The plain of the initial velocities, (v_{inn}, v_{out}), was divided into three regions, see Fig. 11. In the regions A and B (blue and yellow portions, respectively) the difference in velocities v_{inn} and v_{out} is not significant. In the region A, initial energy of the three excited atoms, E_0, is not sufficient for the formation of topological defects and only 3 $\times$ 1-focusons (compressive solitons) were excited. Focusons transfer energy but not mass, and after their attenuation ideal crystal structure is completely restored. In the region B, E_0 is sufficiently large for the formation of a three-vacancy and a supersonic 3 $\times$ 1-crowdion which later transforms into subsonic one. The border between the regions A and B in terms of initial energy is at $100 < E_0 < 120$.

More complicated defect structure evolution is observed in the region C (pink portion of Fig. 11). In this region v_{inn} and v_{out} are noticeably different. We have demonstrated that the energy exchange between the outer rows and the inner row takes place and it becomes very important when the difference between v_{inn} and v_{out} is prominent. Due to the difference in the initial velocities, point defects can appear already for $E_0 = 50$, which is considerably smaller then the energy threshold formation for the region B. However, for relatively small E_0 number of emerging Frenkel pairs in the region C is less than three.

Another important manifestation of the large difference between v_{inn} and v_{out} is the appearance of a vacancy in the inner row dozens of interatomic distances away from the initiation point. It seems that the vacancy moves long distances at supersonic speeds. The mechanism of such counter-intuitive vacancy motion was described by introducing the notion of extended vacancy or voidion, see Fig. 12).

Hence the two main findings can be formulated as follows. When the difference between v_{inn} and v_{out} is large,

- topological defects can appear in the lattice at much lower initial energy E_0;
- a vacancy can appear dozens of interatomic distances away from the initiation point through the formation of a voidion.

These results are important because they reveal new mechanisms of mass transfer in nonlinear lattices.

No doubt that the mechanism of voidion formation and relaxation discussed here for a 2D nonlinear lattice can be realized in the crystal lattices of metals [33], and this is the subject for future works. The effect of temperature on crowdion dynamics is an important issue [32]. In this study, we were dealing with a model crystal, but in future studies of metallic materials, the effect of temperature should be discussed.

Declaration of Competing Interest

The authors declare that they have no known competing financial interests or personal relationships that could have appeared to influence the work reported in this paper.

CRediT authorship contribution statement

I.A. Shepelev: Visualization, Investigation. **S.V. Dmitriev:** Conceptualization, Methodology, Software. **A.A. Kudreyko:** Software, Validation. **M.G. Velarde:** Supervision. **E.A. Korznikova:** Data curation, Writing - original draft.

Acknowledgements

I.A.Sh. acknowledges the financial support from the Russian Science Foundation, grant No. 19-72-00109 (obtaining of results, analysis of simulation results). E.A.K. thanks for the financial support the Council of the President of the Russian Federation for state support of young Russian scientists, grant No. MD-3639.2019.2 (writing the manuscript). S.V.D. acknowledges the support of the Russian Foundation for Basic Research, Grant No. 19-02-00971 (discussion of the results). The work was partly supported by the State assignment of IMSP RAS.

References

[1] Balogh Z, Schmitz G. Diffusion in metals and alloys. Phys Metall (Fifth Edition) 2014;1:387–559. doi:10.1016/B978-0-444-53770-6.00005-8.
[2] Seeger A. The mechanisms of diffusion in metals and alloys. J Less-Common Metals 1972;28(2):387–418. doi:10.1016/0022-5088(72)90135-X.
[3] Mehrer H. Diffusion in solids: fundamentals, methods, materials, diffusion–controlled processes. Springer-Verlag, Berlin; 2007.
[4] Natsik V, Smirnov S. Dislocations and crowdions in two-dimensional crystals. Part III: plastic deformation of the crystal as a result of defect movement and defect interaction with the field of elastic stresses. Low Temp Phys 2016;42:207. doi:10.1063/1.4945583.
[5] Kiritani M. Similarity and difference between fcc, bcc and hcp metals from the view point of point defect cluster formation. J Nucl Mater 2000;276:41–9. doi:10.1016/S0022-3115(99)00167-1.
[6] Salehinia I, Bahr D. The impact of a variety of point defects on the inception of plastic deformation in dislocation-free metals. Scr Mater 2012;66:339. doi:10.1016/j.scriptamat.2011.11.028.
[7] Kononenko V, Bogdanov V, Turenko A, Volosyuk M, Volosyuk A. The role of crowdion mass transfer in relaxation processes near hard concentrators. Probl At Sci Technol 2016;104:15–21.
[8] Korbel A, Bochniak W. Stratified plastic flow in metals. Int J Mech Sci 2017;128–129:269. doi:10.1016/j.ijmecsci.2017.04.006.
[9] Terentyev DA, Klaver TPC, Olsson P, Marinica M-C, Willaime F, Domain C, et al. Self-trapped interstitial-type defects in iron. Phys Rev Lett 2008;100:145503. doi:10.1103/PhysRevLett.100.145503.
[10] Paneth HR. The mechanism of self-diffusion in alkali metals. Phys Rev 1950;80(4):708–11. doi:10.1103/PhysRev.80.708.
[11] Dudarev SL, Ma P-W. Elastic fields, dipole tensors, and interaction between self-interstitial atom defects in bcc transition metals. Phys Rev Mater 2018;2:033602. doi:10.1103/PhysRevMaterials.2.033602.
[12] Dudarev S. Density functional theory models for radiation damage. Annu Rev Mater Res 2013;43(1):35–61. doi:10.1146/annurev-matsci-071312-121626.
[13] Derlet P, Nguyen-Manh D, Dudarev S. Multiscale modeling of crowdion and vacancy defects in body-centered-cubic transition metals. Phys Rev B 2007;76(5):054107. doi:10.1103/PhysRevB.76.054107.
[14] Zhang Y, Schwen D, Zhang Y, Bai X-M. Effects of oversized tungsten on the primary damage behavior in Fe-W alloys. J Alloys Compd 2019;794:482–90. doi:10.1016/j.jallcom.2019.04.278.
[15] Domnguez-Gutirrez F, Byggmstar J, Nordlund K, Djurabekova F, von Toussaint U. On the classification and quantification of crystal defects after energetic bombardment by machine learned molecular dynamics simulations. Nucl Mater Energy 2020;22:100724. doi:10.1016/j.nme.2019.100724.
[16] Bhardwaj U, Sand AE, Warrier M. Classification of clusters in collision cascades. Comput Mater Sci 2020;172:109364. doi:10.1016/j.commatsci.2019.109364.
[17] Archilla J, Kosevich Y, Jimnez N, Snchez-Morcillo V, Garca-Raffi L. A supersonic crowdion in mica - ultradiscrete kinks with energy between 40K recoil and transmission sputtering. Springer Ser Mater Sci 2015;221:69–96. doi:10.1007/978-3-319-21045-2_3.
[18] Yang Z, Ma S, Hu Q, Ye H, Chisholm M. Direct observation of solute interstitials and their clusters in Mg alloys. Mater Charact 2017;128:226–31. doi:10.1016/j.matchar.2017.04.003.

[19] Osetsky Y, Bacon D, Serra A, Singh B, Golubov S. One-dimensional atomic transport by clusters of self-interstitial atoms in iron and copper. Philos Mag 2003;83:61–91. doi:10.1080/0141861021000016793.

[20] Matsukawa Y, Zinkle S. One-dimensional fast migration of vacancy clusters in metals. Science 2007;318(5852):959–62. doi:10.1126/science.1148336.

[21] Dudarev SL. Coherent motion of interstitial defects in a crystalline material. Philos Mag 2003;83(31–34):3577–97. doi:10.1080/14786430310001599388.

[22] Dudarev S, Mason D, Tarleton E, Ma P-W, Sand A. A multi-scale model for stresses, strains and swelling of reactor components under irradiation. Nucl Fusion 2018;58(12):126002. doi:10.1088/1741-4326/aadb48.

[23] Balokhonov R, Romanova V, Batukhtina E, Sergeev M, Emelianova E. A numerical study of the microscale plastic strain localization in friction stir weld zones. Facta Univ Ser MechEng 2018;16(1):77–86. doi:10.22190/FUME180102012B.

[24] Popov V. Generalized Archard law of wear based on Rabinowicz criterion of wear particle formation. Facta Univ Ser MechEng 2019;17(1):39–45. doi:10.22190/FUME190112007P.

[25] Chen H-Y, Tsou N-T. The analysis of thermal-induced phase transformation and microstructural evolution in Ni-Ti based shape memory alloys by molecular dynamics. Comput Model Eng Sci 2019;120(2):319–32. doi:10.32604/cmes.2019.06447.

[26] Dmitriev S, Medvedev N, Chetverikov A, Zhou K, Velarde M. Highly enhanced transport by supersonic N-crowdions. Physica Status Solidi Rapid Res Lett 2017;11(12). doi:10.1002/pssr.201700298.

[27] Dmitriev S, Korznikova E, Chetverikov A. Supersonic N-crowdions in a two-dimensional Morse crystal. J Exp Theor Phys 2018;126(3):347–52.

[28] Korznikova E, Sunagatova I, Bayazitov A, Semenov A, Dmitirev S. Effect of interatomic potentials on mass transfer by supersonic 2-crowdions. Lett Mater 2019;9(4):386–90. doi:10.22226/2410-3535-2019-4-386-390.

[29] Shepelev I, Korznikova E, Bachurin D, Semenov A, Chetverikov A, Dmitriev S. Supersonic crowdion clusters in 2D Morse lattice. Phys Lett Sec A 2020;384(1).

[30] Moradi Marjaneh A, Saadatmand D, Evazzade I, Babicheva R, Soboleva E, Srikanth N, et al. Mass transfer in the Frenkel-Kontorova chain initiated by molecule impact. Phys Rev E 2018;98(2):023003.

[31] Bayazitov A, Dmitriev S, Zakharov P, Shepelev I, Fomin S, Korznikova E. Features of mass transfer by N-crowdions in fcc Ni3Al lattice. IOP Conf Ser Mater SciEng 2019;672(1):012033. doi:10.1088/1757-899X/672/1/012033.

[32] Babicheva R, Evazzade I, Korznikova E, Shepelev I, Zhou K, Dmitriev S. Low-energy channel for mass transfer in Pt crystal initiated by molecule impact. Comput Mater Sci 2019;163:248–55.

[33] Iskandarov A, Medvedev N, Zakharov P, Dmitriev S. Crowdion mobility and self-focusing in 3D and 2D nickel. Comput Mater Sci 2009;47(2):429–31. doi:10.1016/j.commatsci.2009.09.004.

[34] Terentyev DA, Malerba L, Hou M. Dimensionality of interstitial cluster motion in bcc-Fe. Phys Rev B 2007;75(10):104108. doi:10.1103/PhysRevB.75.104108.

[35] Koch V, Majumder A, Wang X-N. Cherenkov radiation from jets in heavy-ion collisions. Phys Rev Lett 2006;96(17):172302. doi:10.1103/PhysRevLett.96.172302.

[36] Chetverikov A, Shepelev I, Korznikova E, Kistanov A, Dmitriev S, Velarde M. Breathing subsonic crowdion in Morse lattices. Comput Condens Matter 2017.

[37] Korznikova E, Shepelev I, Chetverikov A, Dmitriev S, Fomin S, Zhou K. Dynamics and stability of subsonic crowdion clusters in 2D Morse crystal. J Exp Theor Phys 2018;127(6):1009–15.

[38] Korznikova E, Shepelev I, Chetverikov A, Fomin S, Dmitriev S. Subsonic M,N-crowdions in 2D Morse crystal. IOP Conf Ser Mater SciEng 2018;447(1):012030. doi:10.1088/1757-899X/447/1/012030.

[39] Mazilova T, Sadanov E, Voyevodin V, Ksenofontov V, Mikhailovskij I. Impact-induced concerted mass transport on W surfaces by a voidion mechanism. Surf Sci 2018;669:10–15. doi:10.1016/j.susc.2017.11.002.

[40] van der Meer B, van Damme R, Dijkstra M, Smallenburg F, Filion L. Revealing a vacancy analog of the crowdion interstitial in simple cubic crystals. Phys Rev Lett 2018;121(25):258001. doi:10.1103/PhysRevLett.121.258001.

[41] Chen Z, Ghoniem N. Biaxial strain effects on adatom surface diffusion on tungsten from first principles. Phys Rev B 2013;88(3):035415. doi:10.1103/PhysRevB.88.035415.

[42] Kedharnath A, Kapoor R, Sarkar A. Atomistic simulation of interaction of collision cascade with different types of grain boundaries in alpha-Fe. J Nucl Mater 2019;523:444–57. doi:10.1016/j.jnucmat.2019.06.021.

[43] Rosandi Y, Urbassek H. The sputter cross section of a surface-vacancy island. Nucl Instrum Meth B 2011;269(14):1619–24. doi:10.1016/j.nimb.2010.12.043.

[44] Krylova K, Korznikova E, Semenov A, Bachurin D, Dmitriev S. Linking tracks in mica crystals with phase transitions in a bistable lattice. Eur Phys J B 2020;93(2). doi:10.1140/epjb/e2020-100565-0.

[45] Bajars J, Eilbeck J, Leimkuhler B. Nonlinear propagating localized modes in a 2D hexagonal crystal lattice. Physica D 2015;301–302:8–20. doi:10.1016/j.physd.2015.02.007.

[46] Bajars J, Chris Eilbeck J, Leimkuhler B. Numerical simulations of nonlinear modes in mica: past, present and future. Springer Ser Mater Sci 2015;221:35–67. doi:10.1007/978-3-319-21045-2_2.

[47] Wattis J, Alzaidi A. Asymptotic analysis of breather modes in a two-dimensional mechanical lattice. Physica D 2020;401. doi:10.1016/j.physd.2019.132207.

[48] Bachurina O. Plane and plane-radial discrete breathers in fcc metals. Modell Simul Mater Sci Eng 2019;27(5). doi:10.1088/1361-651X/ab17b7.

[49] Chetverikov A, Ebeling W, Schll E, Velarde M. Nonlinear excitations and bound states of electrons, holes and solitons in bilayers of triangular lattices. Eur Phys J B 2019;92(6). doi:10.1140/epjb/e2019-90715-8.

[50] Kuzkin V. Thermal equilibration in infinite harmonic crystals. Continuum Mech Thermodyn 2019;31(5):1401–23. doi:10.1007/s00161-019-00758-2.

[51] Chetverikov A, Ebeling W, Velarde M. Localized nonlinear, soliton-like waves in two-dimensional anharmonic lattices. Wave Mot 2011;48(8):753–60. doi:10.1016/j.wavemoti.2011.04.005.

[52] Law K, Kevrekidis P, Koukouloyannis V, Kourakis I, Frantzeskakis D, Bishop A. Discrete solitons and vortices in hexagonal and honeycomb lattices: existence, stability, and dynamics. Phys Rev E 2008;78(6). doi:10.1103/PhysRevE.78.066610.

[53] Rysaeva L, Korznikova E, Murzaev R, Abdullina D, Kudreyko A, Baimova J, et al. Elastic damper based on the carbon nanotube bundle. Facta Univ Ser Mech Eng 2020;18(1):1–12. doi:10.22190/FUME200128011R.

[54] Girifalco L, Weizer V. Application of the Morse potential function to cubic metals. Phys Rev 1959;114(3):687–90. doi:10.1103/PhysRev.114.687.

[55] Ziegenhain G, Hartmaier A, Urbassek H. Pair vs many-body potentials: influence on elastic and plastic behavior in nanoindentation of fcc metals. J Mech Phys Solids 2009;57(9):1514–26. doi:10.1016/j.jmps.2009.05.011.

[56] Semoto T, Tsuji Y, Yoshizawa K. Molecular understanding of the adhesive force between a metal oxide surface and an epoxy resin. Journal of Physical Chemistry C 2011;115(23):11701–8. doi:10.1021/jp202785b. Cited By 66

[57] Costa Filho R, Alencar G, Skagerstam B-S, Andrade J. Morse potential derived from first principles. EPL 2013;101(1). doi:10.1209/0295-5075/101/10009.

[58] Elkhateeb M, Shin Y. Molecular dynamics-based cohesive zone representation of Ti6Al4V/TiC composite interface. Mater Des 2018;155:161–9. doi:10.1016/j.matdes.2018.05.054.

[59] Galashev A, Katin K, Maslov M. Morse parameters for the interaction of metals with graphene and silicene. Phys Lett Sect A 2019;383(2–3):252–8. doi:10.1016/j.physleta.2018.10.025.

[60] Betermin L. Minimizing lattice structures for Morse potential energy in two and three dimensions. J Math Phys 2019;60(10):102901. doi:10.1063/1.5091568.

[61] Chistyakova N, Tran T. A study of the applicability of different types of interatomic potentials to compute elastic properties of metals with molecular dynamics methods. AIP Conf Proc 2016;1772:060019. doi:10.1063/1.4964599.

[62] Hao ZP, Cui RR, Fan YH, Lin JQ. Diffusion mechanism of tools and simulation in nanoscale cutting the Ni–Fe–Cr series of nickel-based superalloy. Int J Mech Sci 2019;150:625–36. doi:10.1016/j.ijmecsci.2018.10.058.

[63] Bai L, Srikanth N, Korznikova E, Baimova J, Dmitriev S, Zhou K. Wear and friction between smooth or rough diamond-like carbon films and diamond tips. Wear 2017;372–373:12–20.

[64] Ikeda K, Doi Y, Feng B-F, Kawahara T. Chaotic breathers of two types in a two-dimensional Morse lattice with an on-site harmonic potential. Physica D 2007;225(2):184–96. doi:10.1016/j.physd.2006.10.017.

[65] Plimpton S. Fast parallel algorithms for short-range molecular dynamics. J Comput Phys 1995;117(1):1–19. doi:10.1006/jcph.1995.1039.

[66] Fitzgerald SP. Structure and dynamics of crowdion defects in bcc metals. J Micromech Mol Phys 2018;03(03n04):1840003. doi:10.1142/S2424913018400039.